Electrostatic Force Microscopy of Electrospun Polymer Nanofibers with Embedded Carbon Nanotubes

Joseph Rahamim

May 10, 2013

Contents

List of Figures

Acknowledgments

I would like to thank my thesis advisor Professor Cristian Staii for his hard work, care and guidance during this project. I'd also Like to thank Professor Peggy Cebe for her help in providing access to resources, and providing information on polymers and electrospinning, and Bin Mao and Yahze Zhu for creating the samples used in this project. Finally I'd like to thank Christopher Kehayias, Daniel Rizzo and Elise Spedden for all their advice during the course of the thesis.

Chapter 1

Introduction

1.1 Motivation

Carbon Nanotubes (CNTs) are long hollow tubes of carbon arranged in a lattice, and exhibit excellent thermal and electrical conductivity, as well as impressive mechanical qualities [1]. This is one of the reasons that CNTs have been heavily researched for possible mechanical applications. Unfortunately CNT's tend to bunch parallel to one another due to van-der-Walls forces which give rise to CNT 'bundles'. Due to the relative ease of overcoming the inter-tube forces these bundles do not exhibit the superior mechanical properties their constituents do [2].

A solution to this that has been explored over the years is to coat the CNT's in a polymer lining. Many different processes have been used to generate such materials such as melt mixing or extrusion [3], and a highly successful approach in recent years has been to produce the CNT-Polymer system by electrospinning a solution/dispersion of the two. A further advantage of such coated CNT's is that it brings the nano-scale structures closer to the macro-scale so that their properties can be utilized more easily for practical purposes [2].

Such a system of CNTs embedded in electrospun polymer nanofibers is rather complex, and a lot of research has gone into understanding its various characteristics [2]. One characteristic of interest would be the dielectric constant of the combined system, given the varying properties of the polymer and CNTs, as well as their distribution. Many techniques to determine the dielectric constant would return data averaged over the length of the fibers and it is in this light that Electrostatic Force Microscopy (EFM) becomes a good option for such measurements. Due to the probing nature of the equipment, measurements of the electrical characteristics of the fiber can be performed on specific locations along the fiber, letting one examine how the dielectric constant changes along parts of the fibers with different diameters, densities of CNTs and distribution of CNTs etc.

1.2 Overview

In order to study the electric characteristics of polymer nanofibers with embedded nanotubes, Electrostatic Force Microscopy (EFM) was conducted on both embedded nanofibers and neat polymer nanofibers. This project studies electrospun nanofibers of polylactic acid (PLLA) with embedded multiwall nanotubes, as well as the case without nanotubes, using techniques in atomic force microscopy (AFM).

The distribution of fibers spun on a silicon substrate is observed by means of an optical microscope. The topography of the nanofibers is then studied using AC mode AFM, and physical characteristics such as the distribution of fiber diameters are studied. Next, electrostatic force microscopy (EFM) is used to measure the dielectric properties of the fibers, and using some modeling of the tip-substrate system, a value for the dielectric constant of the fibers is measured, however the model is found not to apply.

Accurate knowledge of the AFM-tip physical parameters (such as tip radius, spring constant etc.) is required for precise measurement of fiber dielectric constants. To achieve this, a novel technique is explored to find the tip/cantilever spring constant.

Finally deviations from the modeled tip-sample interactions as proposed by this paper are discovered. Transient effects on the cantilever motion as the cantilever measures the edges of fibers breaks the simple harmonic motion analysis employed by AFM. Furthermore, evidence of permanent partial polarization of the dielectric fibers due to the EFM measurement is observed, resulting in long range forces that cause the AFM tip to interact with the fiber even when it is a considerable distance away.

Chapter 2

Background and Experimental Procedures

2.1 Atomic Force Microscopy (AFM)

AFM is a method to image the topography of a sample by studying the effects of inter-molecular forces between a sample surface and a sharp tip, positioned at the end of an oscillating metallic beam, called a cantilever. Since its creation in 1986 [4], AFM has been used to probe a variety of different samples using many different techniques, producing interesting and reliable results.

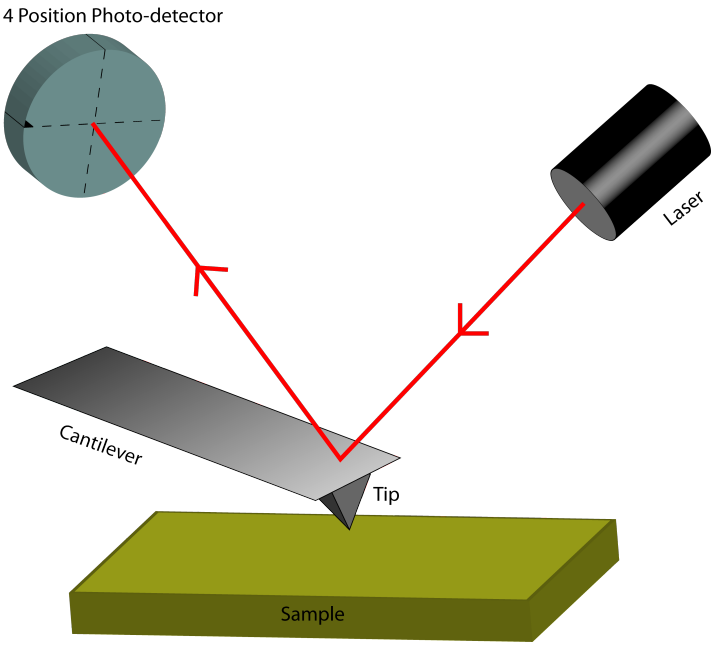

Figure 2.1: The Set Up of the AFM

The set up of the AFM (Fig 2.1) consists of a sharp tip (of typical radius ~50nm) on the end of a cantilever that is held in place. The cantilever can be mechanically oscillated with simple harmonic motion at any acceptable frequency. To track the orientation of the cantilever (when it is being oscillated) a laser beam is reflected off of the back of the cantilever and onto a 4 quadrant photo-detector that can detect the beam's horizontal, as well as vertical displacement. Thus the oscillation of the cantilever can be measured by the AFM.

The general operation of the AFM in tapping (or AC) mode is conducted as follows: The cantilever is driven at a frequency close to its resonant frequency, and it is lowered so that the tip is close to the sample surface to be measured. The sample is then 'raster-imaged'; the tip is moved across the area of the sample sweeping out a line (referred to as the 'Trace') and back again across the same line of motion (referred to as the 'Retrace') recording the oscillation of the cantilever as it goes. Once the tip has swept out a line, it will move down a level and sweep out the next line in the same fashion. It will repeat the process until the entire sample surface has been imaged.

Information about the sample comes from the oscillation of the cantilever as measured by the reflected laser beam on the photo-detector. Far away from the surface of the sample and free from tip-sample interactions, this oscillation should be the same as the driving oscillation. However, if the tip is close to the sample there will be inter tip-sample forces that perturb the actual oscillation of the cantilever away from the driving oscillation. To quantify this effect the actual oscillation of the cantilever is modeled as simple harmonic motion governed by Hooke's Law [4]:

$$F = -kx \tag{2.1}$$

where k is the spring constant of the cantilever and x is the deflection of the cantilever away from its rest position. Thus when the tip is far from the surface of a sample, the cantilever oscillates with simple undamped harmonic motion. However when the tip is close to the sample surface, the tip-sample forces damp the oscillation of the cantilever and its motion is modeled as damped harmonic oscillator.

Thus to understand the topology of a surface, we need to analyze the motion of the cantilever and deduce what tip-sample forces the tip is experiencing, and what sample height that corresponds to. There are a variety of forces between the tip and the sample, broken into two regions. When the tip is close to the sample, the repulsive forces dominate, with coulombic repulsion and the Pauli exclusion principle coming into effect. Further from the sample the tip actually experiences more attractive forces coming from van-der-Walls forces and dipole attraction (Fig 2.2). The tip sample separation determines what the contributions of the forces are to the simple harmonic motion of the cantilever.

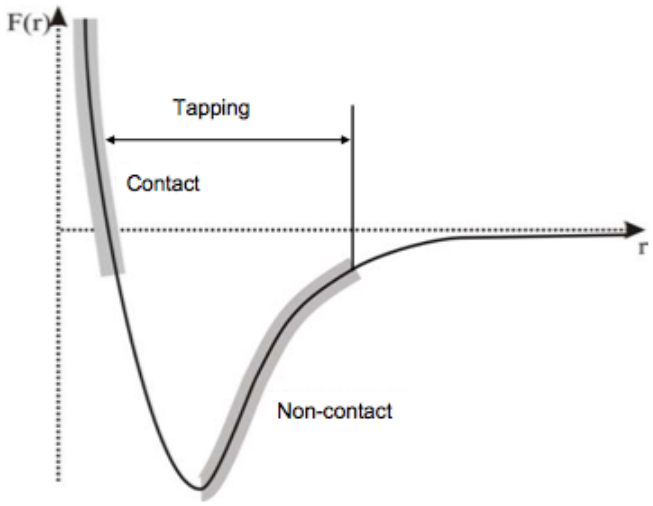

Figure 2.2: A plot of the magnitude of the total tip-sample forces as a function of r, the distance between the tip and the sample. The range of measurement of certain AFM modes is also shown [5].

During tapping mode, the tip experiences both the attractive and repulsive regions of the force curve as it is oscillated above the surface. Initially the cantilever is tuned by the AFM to identify its resonant frequency. The cantilever is then driven at that frequency to achieve a relatively large amplitude (~100nm). As the tip is swept along the surface of the sample, an electronic feedback loop is employed to keep the amplitude of the cantilever oscillation constant. If the tip cantilever is very close to the sample the tip will mostly be in the repulsive regime of the force curve in the course of one oscillation cycle, and its amplitude will be diminished. To compensate for this the cantilever is raised, indicating a increase in height in the surface topography (Fig 2.3). Conversely, if the tip is far from the surface then the overall tip-sample forces will be the long-range, attractive forces, and the cantilever oscillation amplitude will increase, and so the cantilever will be lowered to compensate indicating a lowering in height of the sample topography.

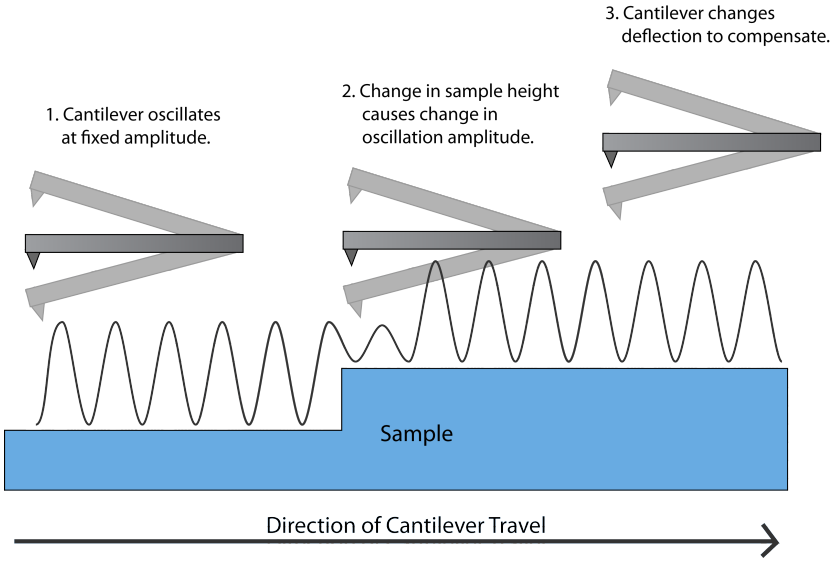

Figure 2.3: *Tapping mode AFM operation*

The advantage of tapping mode measurements as opposed to some other topography measurements such as contact mode is that it minimizes the damage to the sample due to the tip[4].

Further AFM techniques can be employed to manipulate a sample or measure a variety of data other than topography. Electrostatic Force Microscopy is an example of an alternate technique and it is used in this project to study electrostatic characteristics of samples.

2.2 Electrostatic Force Microscopy (EFM)

Electrostatic Force Microscopy is an AFM technique used to measure the distribution of charge in a sample. With suitable modeling it can also be used to measure the dielectric constant of a sample[6]. To perform EFM, a special tip with a conductive coating (such as Ti or Pt) is used.

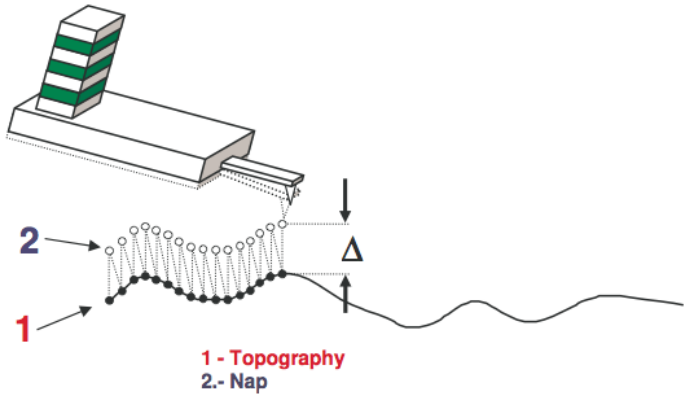

Figure 2.4: The two passes of EFM. On the first pass (1) normal AFM topography is done, on the second (2) EFM is performed at delta height above the sample surface [7].

The method of operation is called a two-pass technique (Fig 2.4). The device raster-images the sample surface as before, except this time it takes two sweeps of each line segment (hence the name two-pass technique). On the first pass, consisting of both trace and retrace, the AFM performs a normal topography scan in tapping mode, thus gathering information about the height of the sample.

On the second pass the AFM tip retraces the topography at a fixed height above the sample (referred to as the delta height), using the topographical data obtained in the first pass. During the second scan a DC voltage bias is applied to the AFM tip. This adds an electrostatic tip-sample force into the factors influencing the cantilever's oscillation. Specifically, it is the force generated by electric charge or electric dipoles in the sample, that are experiencing the electric field generated by the potential on the tip. The electric field between the tip and sample will result in an electrostatic force between the two, which will perturb the motion of the cantilever away from resonance (shift of the resonant frequency to a lower value[6]). The size of the shift in phase between the driven oscillation and the mechanical response depends on the local electrostatic properties (charge distribution, dielectric constant etc.) of the sample.

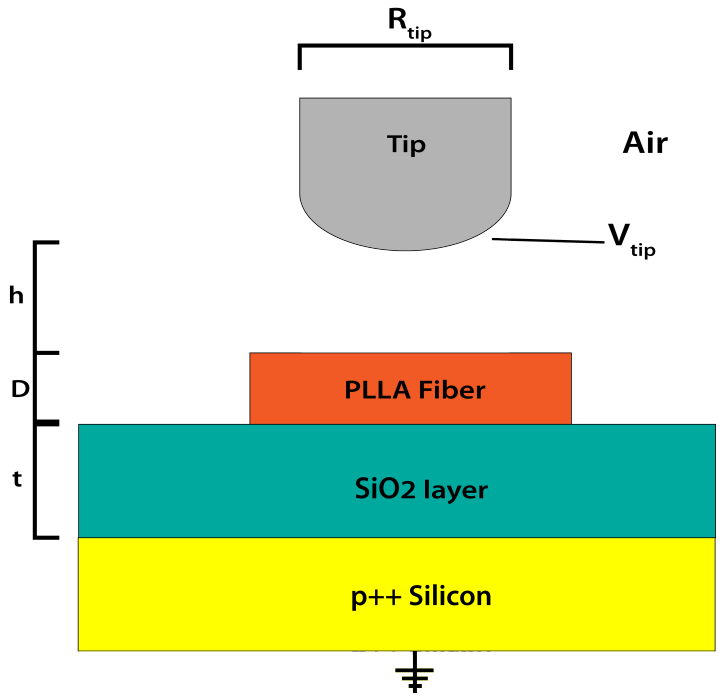

Figure 2.5: Schematic of EFM measurement. Parameters of the measurement are shown visually, t the thickness of the fiber, D the diameter of the fiber, h the delta height of the EFM measurement, V_{tip} the tip voltage and R_{tip}, the radius of the tip. Because the tip diameter is much smaller than the fiber diameter and is in general very close to the surface, the fiber can be modeled as flat in the region of the tip measurement.

To quantify this method, the tip-sample system is treated as a capacitor [8] Fig(2.5). The energy dU required to move an element of charge dq to the positive electrode of a capacitor of potential V is:

$$dU = V dq \tag{2.2}$$

This then allows us to write:

$$V = \frac{q}{C} \tag{2.3}$$

so

$$dU = \frac{q}{C} dq \tag{2.4}$$

$$\Rightarrow \int_0^U dU = \int_0^Q \frac{q}{C} dq = \frac{q^2}{2C} = \frac{1}{2} C V^2 = U \tag{2.5}$$

and we can relate this to the force experienced by the tip by:

$$\vec{F} = -\nabla U \tag{2.6}$$

If the electric field is normal to the surface, then the derivative is simplified to just the derivative in along the normal direction, i.e. the height of the tip above the fiber, h:

$$= -\frac{\partial U}{\partial h} = \frac{1}{2}V^2\frac{\partial C}{\partial h} \tag{2.7}$$

so the force is related to the second derivative of the capacitance:

$$F = \frac{1}{2}V^2\frac{\partial C}{\partial h} \tag{2.8}$$

Now we relate the formula to EFM. The damping forces will cause the resonant frequency of the tip to decrease from the free air resonance. The diagram below shows that this gives a corresponding positive phase shift (Fig 2.6).

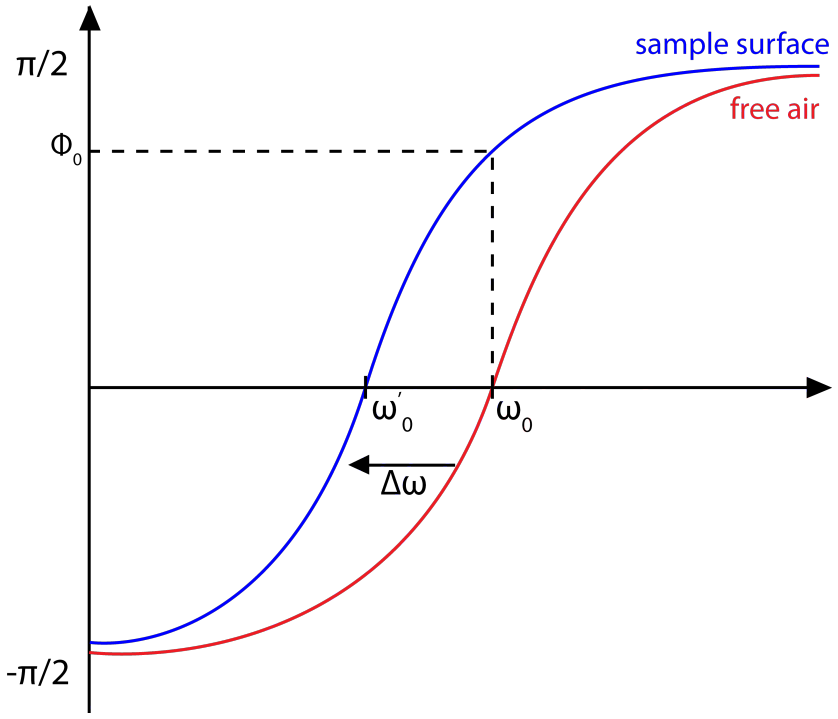

Figure 2.6: A plot of the frequency of the cantilever oscillation against the phase shift of the oscillation in free air (red) and close to the sample surface (blue). When the tip moves close to the sample surface it feels an attractive electrostatic force during EFM. This lowers the resonant frequency of the cantilever away from its free air resonance ω_0 to a lower value $\omega_0^{'}$. So the phase-frequency curve shifts to the blue line. However under EFM the cantilever is still driven at ω_0 so a positive phase shift will be measured as shown by ϕ_0

It can be shown that the phase shift due to electrostatic forces is given by[6]:

$$tan(\phi_0) = \frac{Q}{2k} C^{''}(h) V_{tip}^2 \tag{2.9}$$

where Q is the quality factor of the tip oscillation, k is the tip spring constant and V_{tip} is the voltage on the tip. This shift is produced whenever the tip is close to a surface. Thus we will always measure a base phase shift when performing EFM, given by the tip-substrate background phase. The dielectric properties of a sample (such as polymer fiber on top a SiO_2 substrate) can be extracted by measuring the phase shift above the sample, relative to the background phase recorded above the substrate (e.g. SiO_2).This relationship is given by[6]:

$$tan(\phi) - tan(\phi_0) = -\frac{Q}{2k} \left(C_1^{''}(h) - C_2^{''}(h) \right) V_{tip}^2 \tag{2.10}$$

or for small ϕ and ϕ_0 :

$$tan(\phi - \phi_0) = -\frac{Q}{2k}\left(C_1^{''}(h) - C_2^{''}(h)\right)V_{tip}^2 \tag{2.11}$$

where ϕ_0 is the phase shift measured for just the substrate, and ϕ is the phase shift measured of the sample and substrate combined. Using this we can determine values for the capacitance derivatives. We can use this to experimentally determine the dielectric constant of the sample by making a further assumption that the tip and sample geometry can be modeled as a series of parallel plate capacitors.2.7

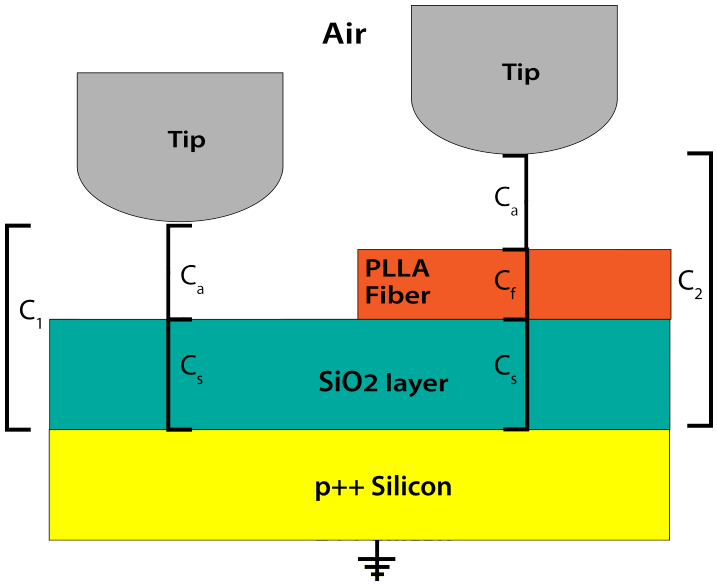

Figure 2.7: The tip fiber system modeled as a series of parallel plate capacitors. Here C_1 is composed of C_a,the capacitor filled with air and C_s, the capacitor filled with substrate. C_2 consists of C_a, C_s and C_f, the capacitor filled with the fiber material. The inverses of the plate capacitances can be summed and differentiated with respect to the tip height h, to get the modeling equations below.2.122.13

This is justified for small tip-sample separations of the order of the tip radius[6]. For the dielectric constant of the substrate we get:

$$C_1^{''}(h) = 2\varepsilon_0\left(\pi R_{tip}^2\right)\frac{1}{\left(h + t/\varepsilon_s\right)^3} \tag{2.12}$$

where R is the radius of the tip, h is the delta scan height, t is the thickness of the silicon dioxide substrate layer and ε_s is the dielectric constant of silicon dioxide. For the sample and substrate combined, we can determine the dielectric constant of the sample with the relationship:

$$C_2^{''}(h) = 2\varepsilon_0\left(\pi R_{tip}^2\right)\frac{1}{\left(h + t/\varepsilon_s + D/\varepsilon_f\right)^3} \tag{2.13}$$

where D is the diameter if the fiber, and ε_f is the dielectric constant of the fiber.

2.3 The Dielectric Constant

The dielectric constant or relative permittivity of a dielectric material is a measure of how susceptible the material is to polarization. The constant is dimensionless, and can be defined as the ratio of the magnitude of the electric field in a vacuum vs the electric field in the dielectric medium:

$$\varepsilon_r = \frac{E_0}{E} \tag{2.14}$$

For materials that have a higher dielectric constant, the constituents of the dielectric are influenced more by the electric field, and the internal electric field created by the polar molecules cancels out more of the external field. Thus the higher the value of ε_r the more the dielectric is susceptible; totally resistant material would have a relative permittivity of 1 whereas a theoretically perfect metal would have a value of infinity.

The dielectric constant is a property of materials that is of particular importance regarding capacitors, and can be defined as the ratio of the capacitance of a parallel plate capacitor in vacuum to the capacitance of the same capacitor filled with the dielectric. Using a dielectric with a higher dielectric constant increases the capacitance as potential is stored in the medium as well as the capacitor plates.

2.4 Electrospun Polymer Fibers

Electrospun polymer fibers are fibers with diameters in the nanoscale range created by the electrospinning process.

The general procedure of electrospinning is achieved by extruding a substance such as a polymer from a solution through a high electric potential onto a target collector (Fig 2.8).

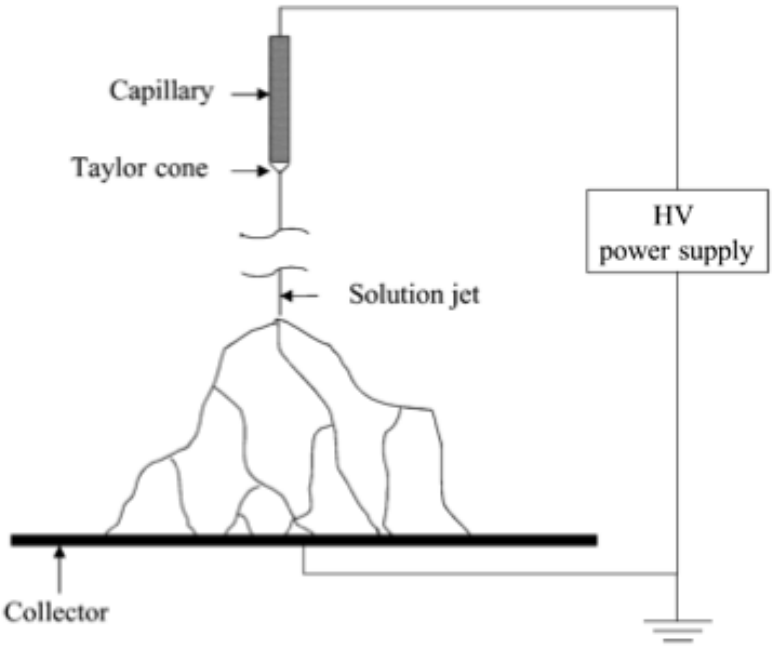

Figure 2.8: Schematic of an electrospinning device. Solution jets leave the capillary and are collected on the grounded collector.[9]

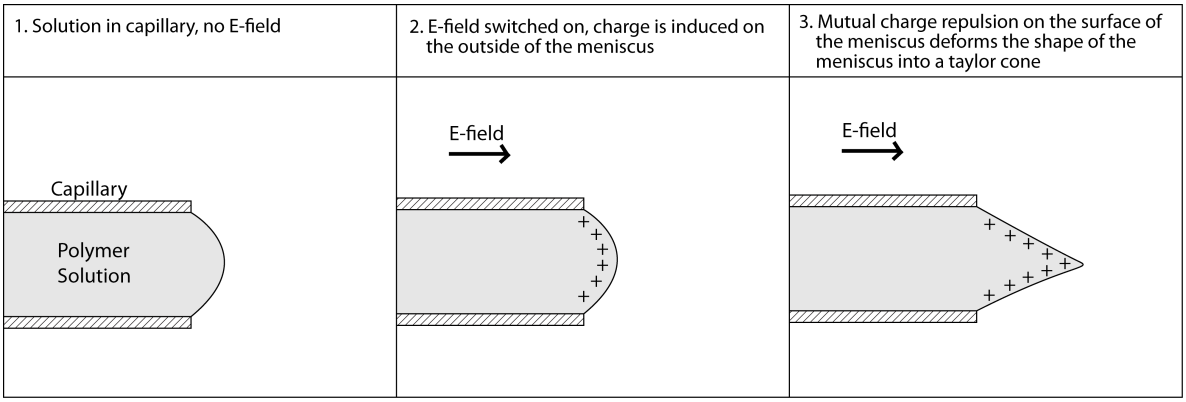

Figure 2.9: Formation of a Taylor cone [10]

The polymer to be spun is first dissolved in an appropriate solution, and then loaded into a capillary such as a syringe. A potential is then put between the end of the capillary tube and the target collector, so that the end of the capillary tube is subject to a strong electric field. The end of the capillary tube is open, and the polymer fluid is held by surface tension. The applied electric field however, induces

charge on the surface of the liquid. The surface charges then repel one another, counteracting the surface tension. As the electric field is increased the hemispherical surface of the fluid at the end of the capillary tube is deformed due to this repulsion, and the shape changes to a cylindrical spike known as a Taylor cone [10] (Fig 2.9). When the increasing electric field reaches a certain critical value, the repulsion of the surface charge overcomes the surface tension and a charged fluid jet is ejected from the capillary towards the target collector. As the jet travels towards the collector the solvent is evaporated off and only the polymer remains. The polymer, now in the shape of a nanofiber due to the extrusion process, is collected on the target.

A number of factors in the electrospinning process can affect the characteristics and shape of the nanofibers [9]. Features like the dimensions of the capillary tube, the strength of the electric field and the rate of flow for fluid samples that are forcefully ejected out of a syringe can impact properties of the fiber such as diameter, cross section, surface topography, production instabilities etc. Electrospinning of fibers is still an active area of research.

2.5 Polylactic Acid

Polylactic acid (PLA) is a thermoplastic polymer composed of two monomers: lactic acid and lactide. It has the chemical formula $(C_3H_4O_2)_n$ and its chemical structure is shown in Fig 2.10

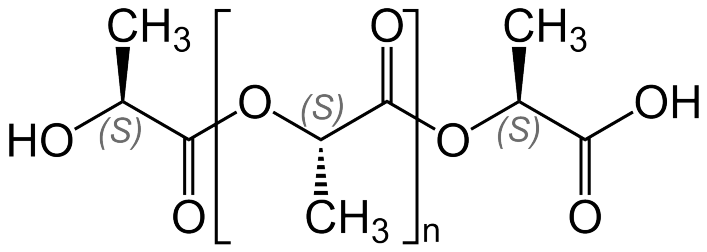

Figure 2.10: The chemical structure of polylactic acid[11]

Lactide comes in two distinct forms, L-lactide and D-lactide corresponding to the chilarity of the molecular structure (Fig 2.11). Both are usable in creating PLA, and the properties of the polymer depend on what mixture of these two monomers was used. For example using an even mixture of both results in PDLLA, which has amorphous qualities. Using pure L-lactide results in PLLA, while pure D-lactide results in PDLA.

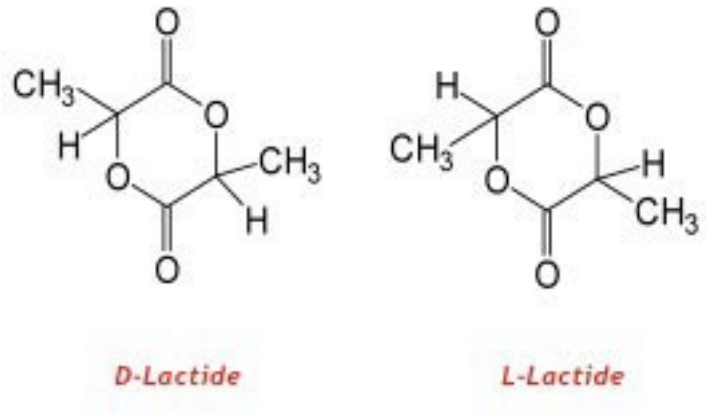

Figure 2.11: The chiral structures of L-lactide and D-lactide[12]

In this project the polymer used was a mixture of PLLA and PDLA, with 96% of the polymer being PLLA and the other 4% being PDLA. Since the polymer is predominantly PLLA, this report will refer to it as such.

2.6 Carbon Nanotubes

A carbon nanotube (CNT) is a hollow cylindrical lattice of carbon atoms that are arranged in a hexagonal pattern. CNT's are known to have good electric and thermal conductivity, as well as superior mechanical properties.[13] The structure of the carbon atoms in the lattice can take on one of three shapes, armchair, zig-zag and chiral (Fig 2.12), and the different shapes give different properties to the resultant CNT. This structuring of the CNT is dependent on the production process in which it was created.

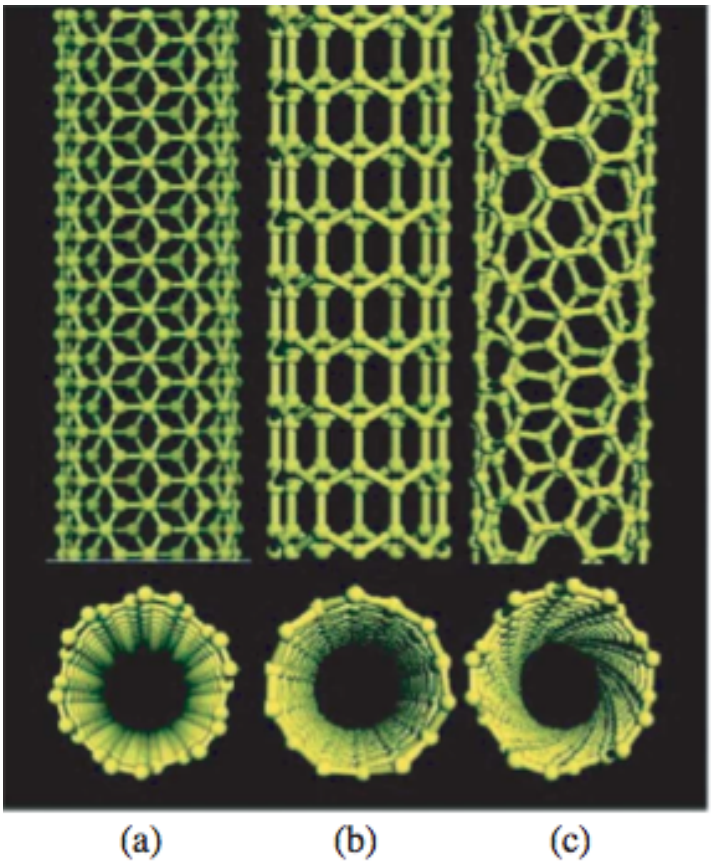

Figure 2.12: The different shapes of a CNT lattice, a) Armchair structure, b) Zig-Zag c) Chiral [2]

On top of these distinctions, CNTs can also be single walled or multi-walled. A single wall nanotube simply consists of one hollow cylindrical tube, and has a typical diameter of 1-2 nanometers. A multi-wall nanotube on the other hand consists of several hollow cylinders nested inside one another, and held in place by intermolecular forces (Fig 2.13). These CNTs can have diameters of up to 100nm [14].

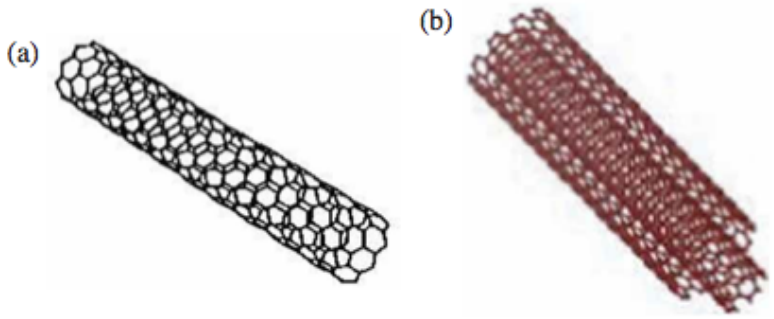

Figure 2.13: CNT structure, a) single wall, b) multi wall [2]

Whilst single wall CNTs can be easily considered as perfect identical molecules of rolled up graphene, multiwall nanotubes on the other hand have larger diameters and lengths of several micrometers. In this light they can be considered as disordered solids, as over long lengths one can expect to find imperfections and adsorbates on the outer most cylinder [15]. These imperfections influence the electronic transport of the system, and intentional manipulations can be performed to achieve specific properties. Multiwall nanotube properties and manipulation are still very active fields of research.

2.7 Experimental Samples

In this experiment the samples consisted of electro-spun fibers of plain polylactic acid (PLLA), as well as PLLA fibers with carbon nanotubes embedded inside of them. The fibers produced were observed to have a smooth topology under AFM, and two general ranges of diameter were found. Larger fibers were created with diameters on the order of 3-4 μm, and smaller fibers were found with diameters between 80-300nm.

Neat PLLA nanofibers, and PLLA nanofibers with CNTs embedded inside (PLLA w/CNT) are the system characterized in this project. The fibers are created by dispersing the CNTs inside the polymer solution that is to be spun by the electrospinning apparatus. The electrospinning produces fibers with embedded CNTs aligned with the fiber axis.[2] During production, when the electric field causes the meniscus on the edge of the capillary to deform into a Taylor cone, the change to the new shape causes flow within the sample along streamlines. The streamlines are along the fiber axis, and the CNTs orient themselves along the streamlines, thus also becoming aligned parallel to the fiber axis. When the solution along with the CNT is ejected from the cone, the strain caused by this process helps to align the CNTs further. The samples were fabricated in Professor Cebe's lab by Bin Mao and Yazhe Zhu. In the electrospinning set up a spinning drum collector was used to get oriented fibers, i.e. fibers with the same fiber axis.

As PLLA was used to create the fibers, the structure of the fibers was anisotropic, that is the chemical structure along the fiber axis differs from the structure perpendicular to the axis. Since AFM measures properties of the fiber that are perpendicular to the fiber axis, we can only measure the perpendicular

or transverse properties of the neat and composite fibers.

2.8 EFM Measurements

Two types of sample were measured in identical ways, the electrospun fibers of the neat polymer (PLLA) and the polymer with embedded CNT's. Both samples were spun onto a silicon dioxide substrate, and then the substrate base was glued to glass slides to prevent drifting of the sample during EFM scanning. For both samples, fibers with approximate diameters of 80-300nm were measured.

EFM was performed on the PLLA and PLLA w/CNT nanofibers, with the first pass performing tapping mode AFM, and the second pass performing actual EFM (section 2.2). EFM was performed at different delta heights of 50 nm, 100 nm 200 nm and 400 nm in order to find a balance between signal and noise. At each delta height EFM was performed for different tip voltages of 0 V, ± 2 V, ± 4 V, ± 6 V, and ± 8 V.

AFM topography data on the tip height, amplitude and phase (during the retrace scan), as well as the tip oscillation phase during EFM (both trace and retrace data) were collected.

Since equation (2.13) is to be used to calculate ε_f, there are parameters that are needed in order to get accurate numerical values of the dielectric constant. Some parameters are constant throughout the entire experiment. These are the radius of the tip (29 nm$\pm$10 nm), according to the manufacturer specifications, the spring constant of the tip (2.0 N/m with range of values 0.5 N/m - 4.0 N/m), the thickness of the SiO_2 substrate layer (200 nm) and the dielectric constant of SiO_2 ($\varepsilon_s = 3.9$).

Other parameters are specific to the fiber being measured. These include the fiber diameter (typically 300nm), the delta height of the measurement and the Quality factor of the tip's oscillatory motion, determined when tuning the AFM and with a typical value of 180.

Chapter 3

Results and Analysis

3.1 Measuring the Tip Spring Constant

3.1.1 Using EFM and the Fiber Dielectric Constant Model

In performing data analysis it was discovered that the equation modeling the dielectric constant of the fiber was very sensitive to the input parameters. In particular Eq (2.10) allows us to form a relationship between the tangent of the phase shift and the tip voltage squared, but in order to calculate $C_2^{''} - C_1^{''}$ we must know parameters of the tip, in particular Q, the quality factor of the tip oscillation and k, the spring constant of the tip. Q is measured by the AFM to a high degree of accuracy when tuning the tip motion at the start of the experiment. This is inferred from repeated measurements of Q for the same tip.

Conversely the value of k was initially taken to be the value provided by the tip manufacturer information, of 2 N/m in the range 0.5-4 N/m. Since the relative spread of values was so high, a method of measuring k was devised. Eq (2.9) gives us a relationship between k and $C_1^{''}$, and Eq (2.12) allows us to calculate a value of $C_1^{''}$ from experimental parameters.

For a given tip, EFM was performed on a bare substrate surface of SiO_2 of thickness 200 nm and with dielectric constant $\varepsilon_s = 3.9$. Scans were done at tip voltages of 0, 2, 4, 6 and 8 V. From a particular image, the mean phase shift can be measured by plotting a histogram of the values of a patch of the scan as shown below.

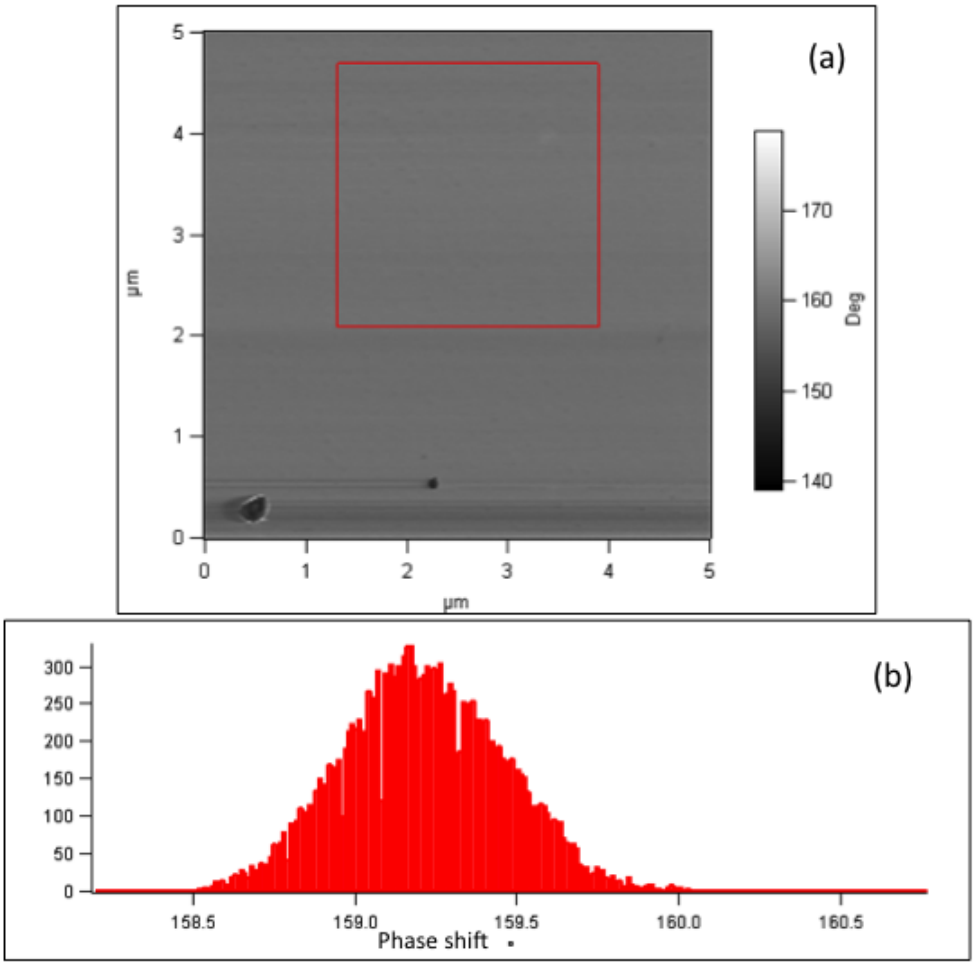

Figure 3.1: a) EFM scan at 4V of the phase of the tip oscillation over SiO_2 substrate with red box marking area of values taken for histogram. b) Histogram of values captured in a) showing a gaussian distribution.

The mean value of the distribution of the histogram can be measured to obtain a value for the phase shift. Doing this for each image allows us to plot $tan(\phi)$ against the tip voltage squared.

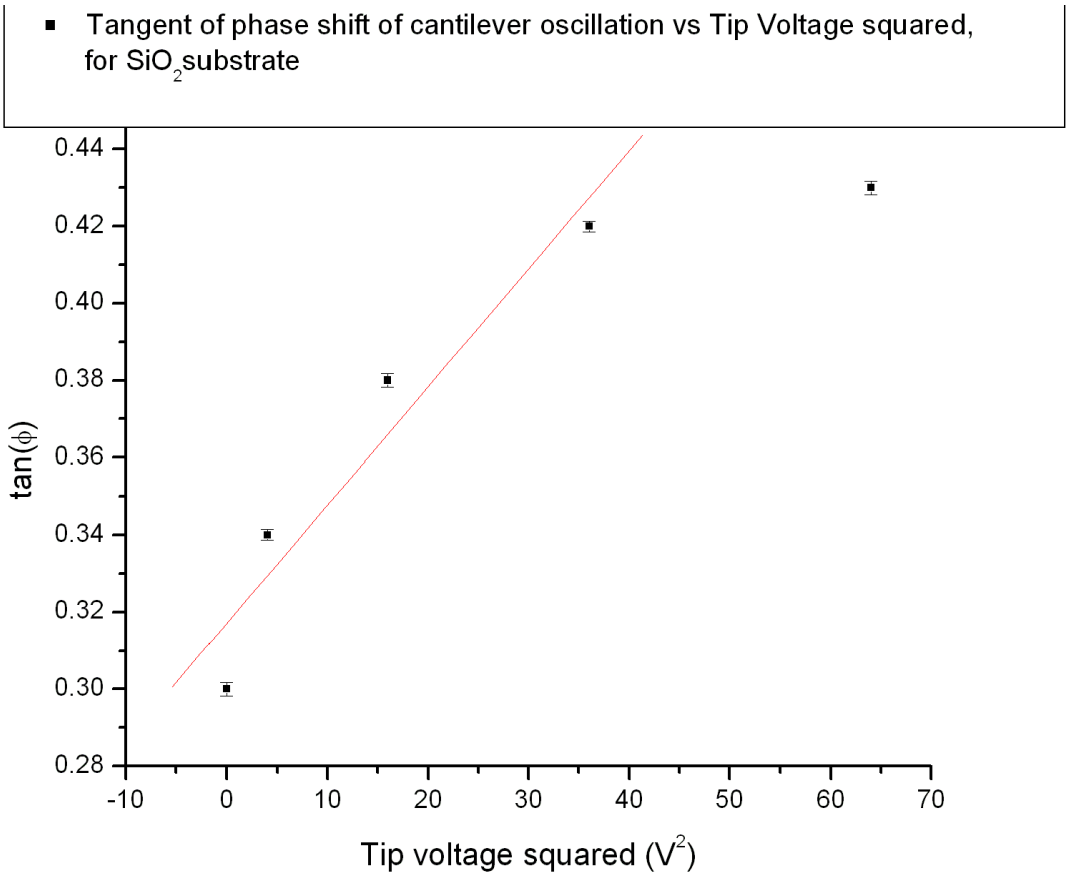

Figure 3.2: A plot of the tangent of the phase shift against tip voltage squared when EFM is performed on SiO_2 substrate. A linear trend is expected from eq(2.9). .

And with Q measured, and C_1'' determined by experimental parameters, k can be measured.

3.1.2 Measuring the Tip's Behavior under Thermal Oscillations

Another, more conventional technique for measuring k using an AFM is to calculate the spring constant by observing the tip motions under Brownian motion. This technique is implemented in the AFM software and the process is outlined here. The first step is to calibrate the sensor signal to the actual force felt by the cantilever. The AFM gets information about the total force experienced by the tip directly from the deflection signal as picked up by the photodetector, and thus outputs a signal in volts. In order to know what force the tip is actually experiencing however, the sensor signal must be calibrated with the actual force experienced by the tip. To achieve this, a single force scan can be carried out whereby the tip is lowered directly onto the substrate. As the tip presses into the surface, the deflection of the tip is measured, providing data to produce a force curve for the tip (Fig 3.3), similar to the theoretical curve presented in Fig (2.2). Assuming the substrate is a theoretically

infinitely hard surface, the AFM uses this curve to correlate the detector voltage signal with the actual force experienced by the tip. In practice a plain glass slide is used as the surface, which has a much higher stiffness than the predominantly silicon tip.

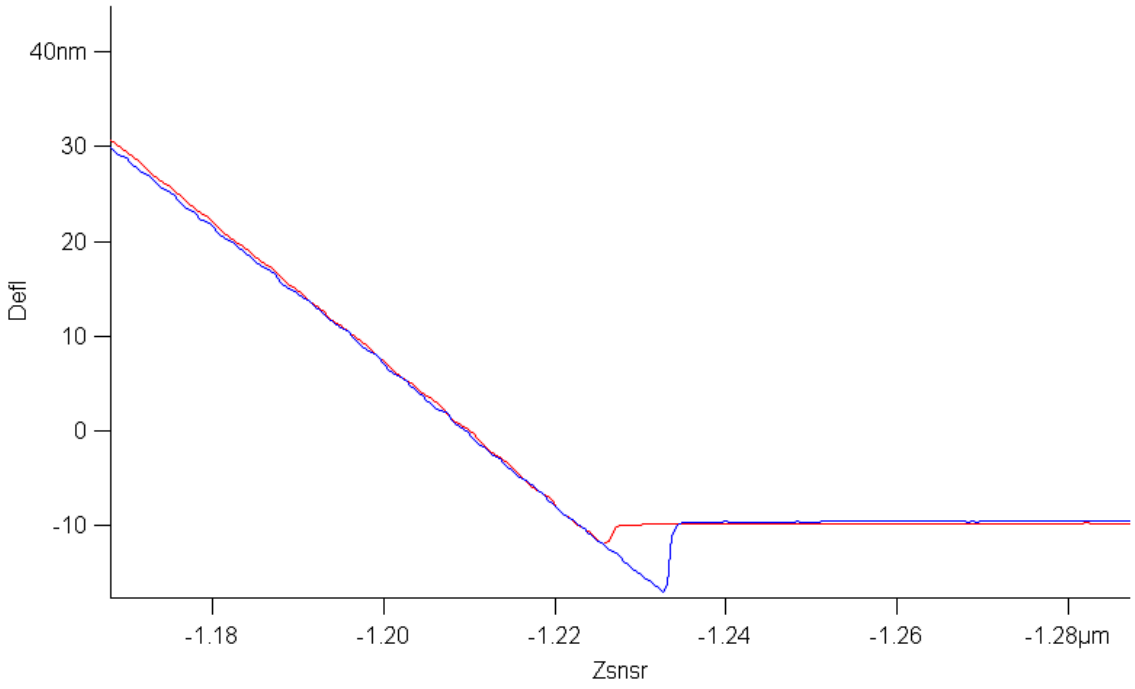

Figure 3.3: The actual force curve of a cantilever as it is pressed into a hard (glass) surface. The x-axis is z-sensor (the elevation of the cantilever above the sample surface) and the y-axis is deflection, which is a measurement of the force on the cantilever.

The next step is to use this information to deduce k by studying the amplitude of oscillation (and thus detector signal) as the cantilever is oscillated at various frequencies. The deflection of the cantilever is observed under thermal oscillations and data is collected on the frequency of the oscillation and the resulting amplitude of the cantilever oscillation. By looking at what frequencies produce the most sizable amplitude of the tip's oscillation the resonant frequency of the tip can be measured, and a resonance curve can be made (Fig 3.4). By fitting a simple harmonic resonance curve to this distribution, the value of the spring constant of the tip can be determined.

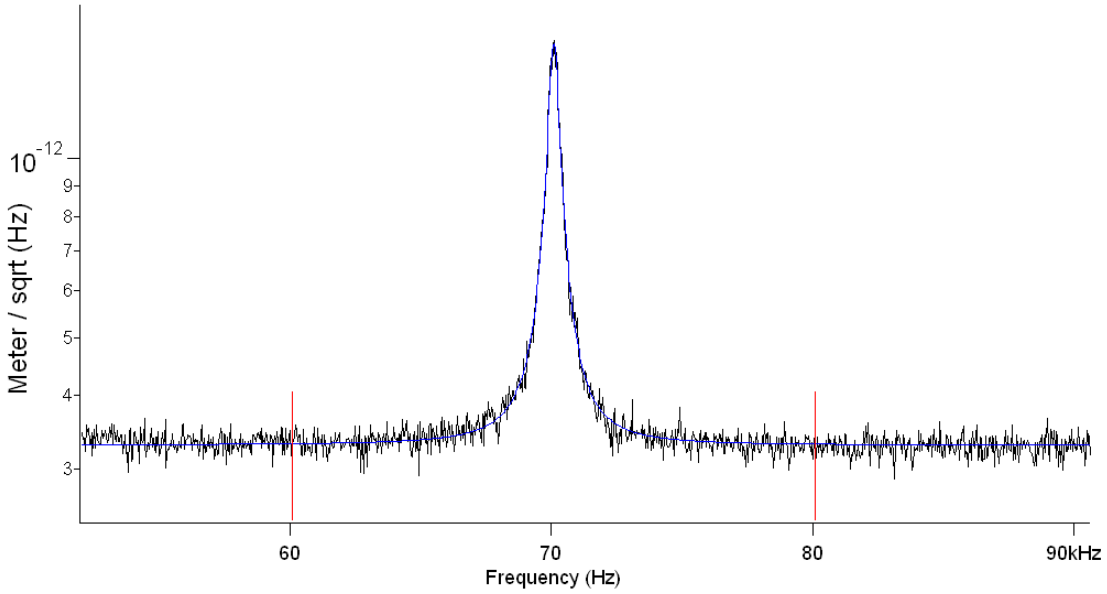

Figure 3.4: The amplitude of cantilever oscillations under thermal vibrations of a spectrum of frequencies. Note the large peak at around 70khz corresponding to the resonant frequency of the cantilever.

Unfortunately the implementation in the AFM software does not return a value for the error of the measurement, so the uncertainties of any values given by this method are unknown.

3.1.3 Comparison of the Two Methods

Both methods were used to determine the spring constant of the same tip. Under the EFM method, the tip constant was found to be 1.0 N/m $\pm$ 0.3N/m; this contrasted with the value of 1.8 N/m determined by the thermal method. Although both values lie within the range of the manufacturer specifications (0.5-4.0 N/m), they differ to a large degree. The value obtained by the EFM method is under further scrutiny as the expected linear relationship is not as strong as hoped (Fig 3.2). For this reason, and because the thermal method is used in other projects, the thermal method was used to determine k in this project.

The advantage of the thermal method is that it is already implemented in the AFM software, and so is much easier to carry out than the EFM method, and takes far less time. The advantages of however is that k can still be inferred retroactively by analyzing areas of substrate in EFM images. This is useful for example if a particular tip breaks and one hasn't measured k yet. Furthermore an error on the measurement can be obtained when using this measurement.

3.2 Deviations from the Simple Model of Tip-Fiber Interactions

EFM measurements showed evidence of phenomena that could not be explained by the simple tip-fiber model that was covered in Section 2.2, and indicated that further modeling would be necessary to fully understand the tip-fiber system. One significant phenomenon was the measurement of positive phase shifts when the tip was near the edges of the fiber (Fig 3.5). These effects have been repeatedly observed in EFM measurements and are often called 'cross-talk'.[16] Physically what occurs here is transient forces as the tip scales the edges of the fiber, which break the oscillation of the tip away from simple harmonic motion. Around the middle of the fiber, we do not expect these transient forces as the fiber topography isn't changing rapidly, so cross-talk is not much of an issue to the measurement of the negative phase shift.

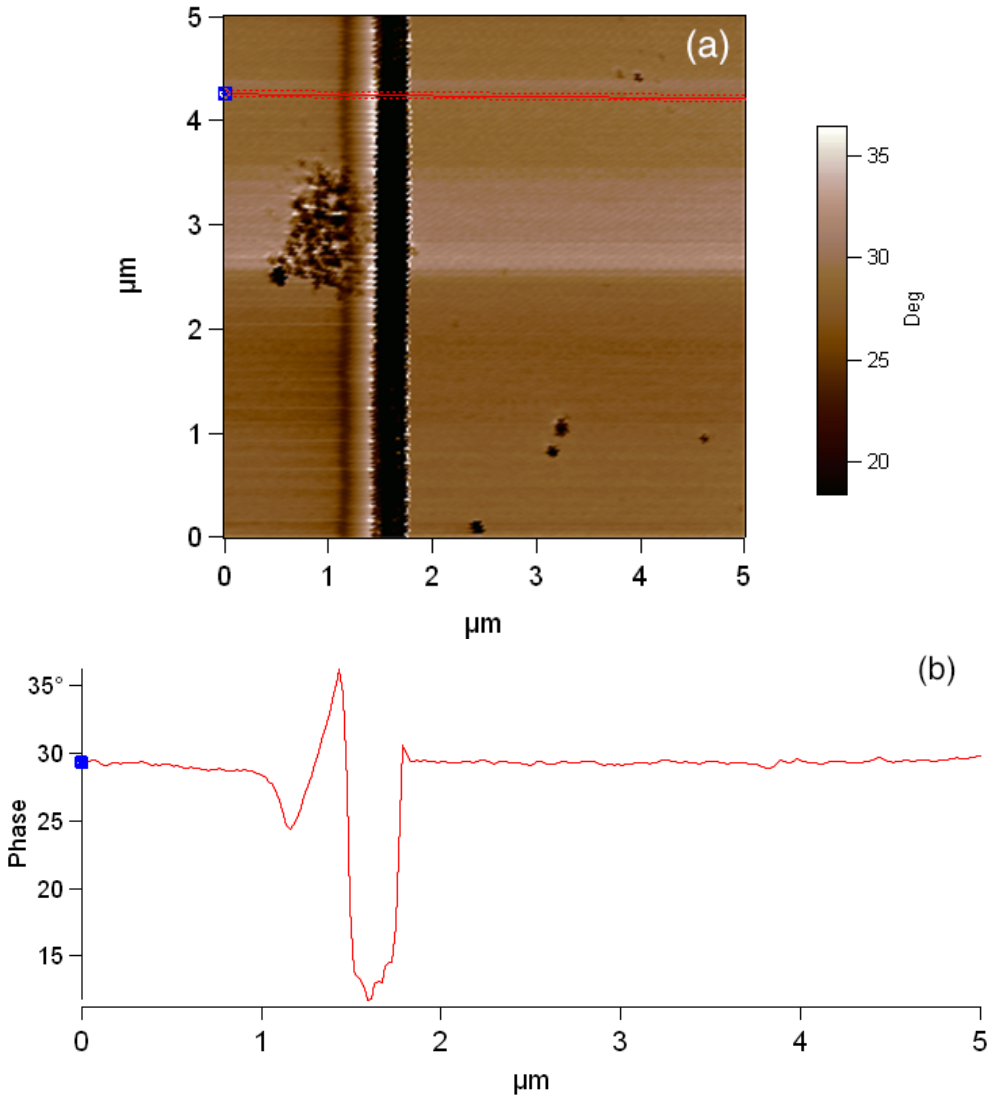

Figure 3.5: a)An EFM retrace phase image of a fiber. The fiber runs through the middle of the image from top to bottom, and is resting on the SiO_2 substrate. A horizontal red line indicates the line cut that was used to produce the adjacent graph. b) A graph of the phase of the tip under EFM of a neat PLLA fiber, across a line segment of the fiber perpendicular to the fiber axis. In the middle of the fiber a negative relative phase shift occurs as predicted by the current tip-fiber model. Near the edges of the fiber however there are positive relative phase shifts indicating cross-talk.

Another, more problematic deviation from the simple model used in this project was a hysteresis in the phase shift as it passed over the fiber. EFM scans of neat PLLA fibers were conducted with tip voltages of +6 V and -6 V. The phase of the oscillation was recorded on both the trace and retrace of the cantilever motion. On trace, the cantilever moves from the left of the fiber to the right measuring phase as it moves. Conversely on retrace the cantilever moves from the right of the fiber to the left. Ideally both measurements would be the same however this is not observed to be the case Fig(3.6).

EFM scans show a baseline value to the left and right of the graphs that give the phase shift of the tip-substrate system, however we find that after measuring the fiber, the tip still feels forces from the fiber and the result is a further negative phase shift, reducing in value as the tip moves away from the fiber and converges back to the baseline value.

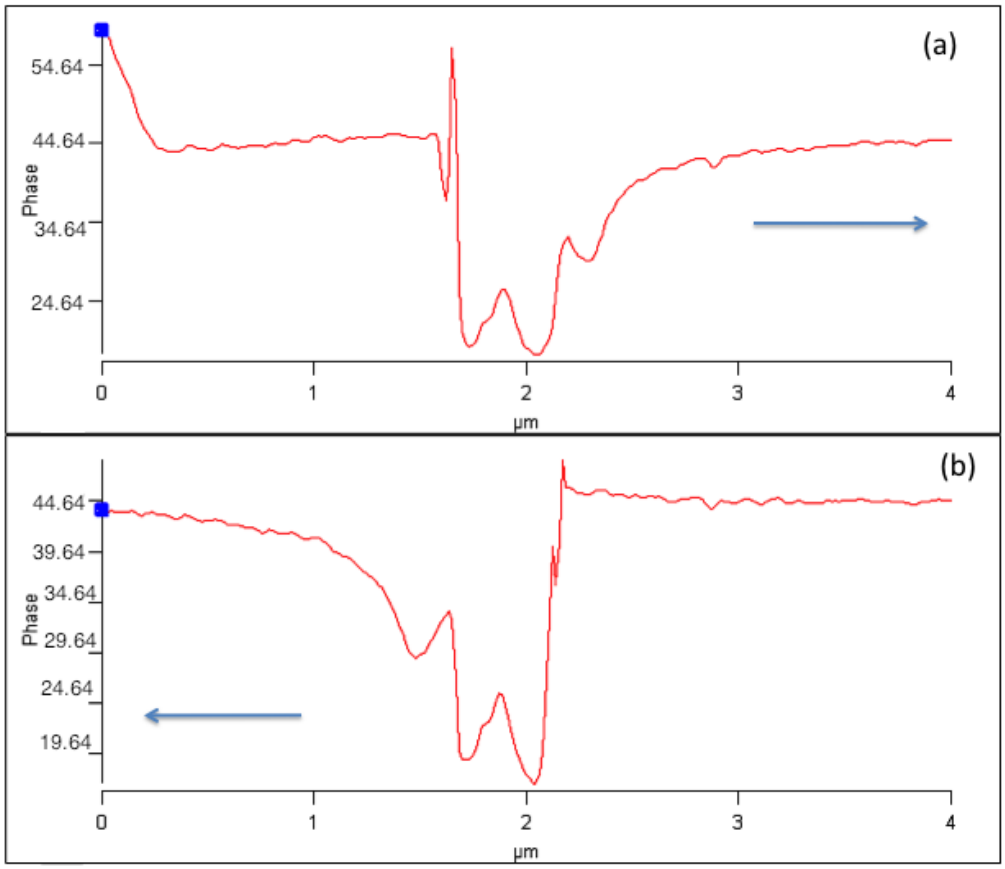

Figure 3.6: a) Trace graph of the phase of the tip oscillation under EFM with tip voltage of 6 V of a neat PLLA fiber, across a line section of the fiber perpendicular to the fiber axis. The direction of the cantilever rastering motion is indicated by an arrow. Note how the right side of the image takes longer to reach the baseline value set by the substrate. The slope on the very left of the image is an artifact of the cantilever being lowered to the surface at the start of the line scan. b) Retrace graph of the phase of the tip oscillation of the same EFM measurement of a neat PLLA fiber, across the same line section. Now it is the left side of the image that takes a longer time to reach the baseline value.

Such an effect can be explained by a permanent partial polarization of the fiber as the tip with a voltage is passed over the fiber surface, resulting in long range electrostatic forces between the fiber and the tip that are experienced by the tip even after moving past the fiber. Interestingly these effects have never been observed before and open up new avenues for research. Such an effect would be complex to model analytically and would have to be studied with numerical simulations.

Interestingly preliminary measurements of a MW CNT embedded PLLA fiber have shown that they do not experience this long range post-fiber interaction Fig(3.7).

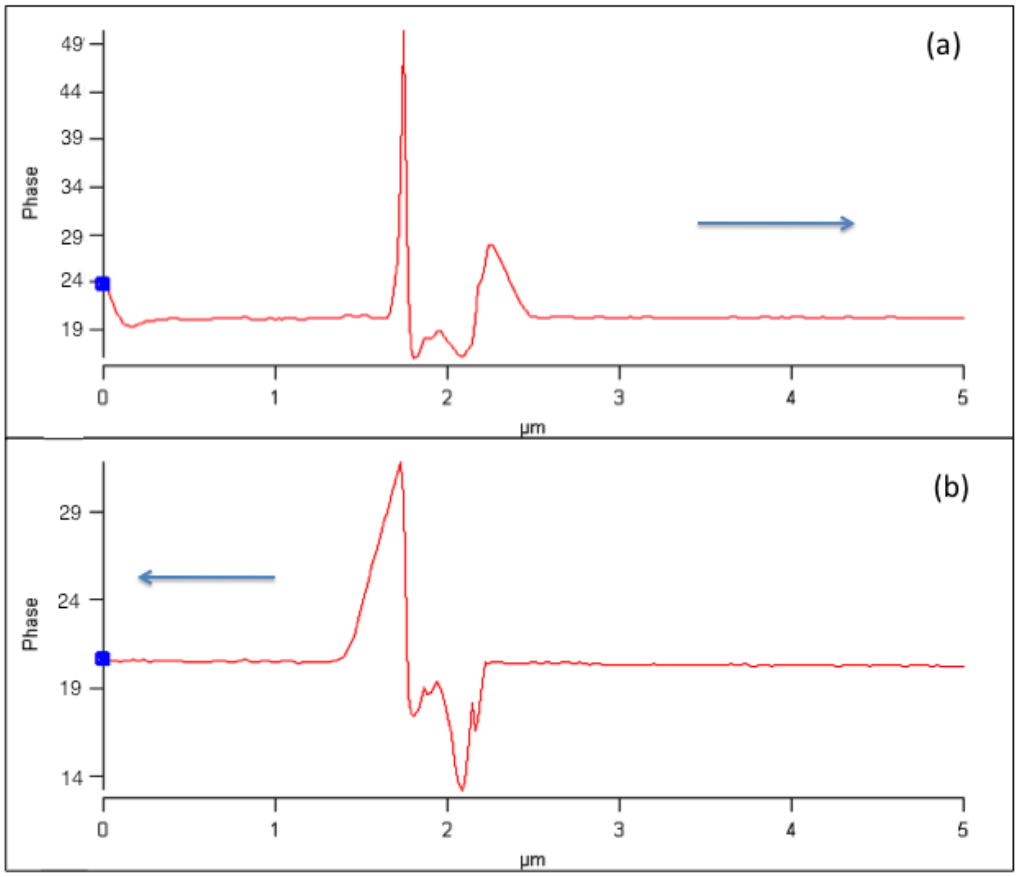

Figure 3.7: a) Trace graph of the phase of the tip oscillation under EFM with tip voltage 6 V of a MW CNT embedded PLLA fiber, across a line section of the fiber perpendicular to the fiber axis. After measuring the fiber (the right most edge of the fiber) the value of the phase returns immediately to the baseline value indicating that there are no long range interactions between the tip and the fiber. b) Retrace graph of the phase of the tip oscillation under the same EFM operation on the same fiber across the same line location. Here too, no interaction is observed past the left most edge.

Analyzing the reason for this would require a deep understanding of the phenomena in the first place as well as an understanding of the electric characteristics of the composite fiber system.

3.3 Neat PLLA Fibers

3.3.1 PLLA Fiber Topography

By way of an optical microscope (3.8), the fibers were revealed to be of varying thicknesses on the micro-scale, with the thickest around 10 µm in diameter and the smallest visible around 0.5 µm.

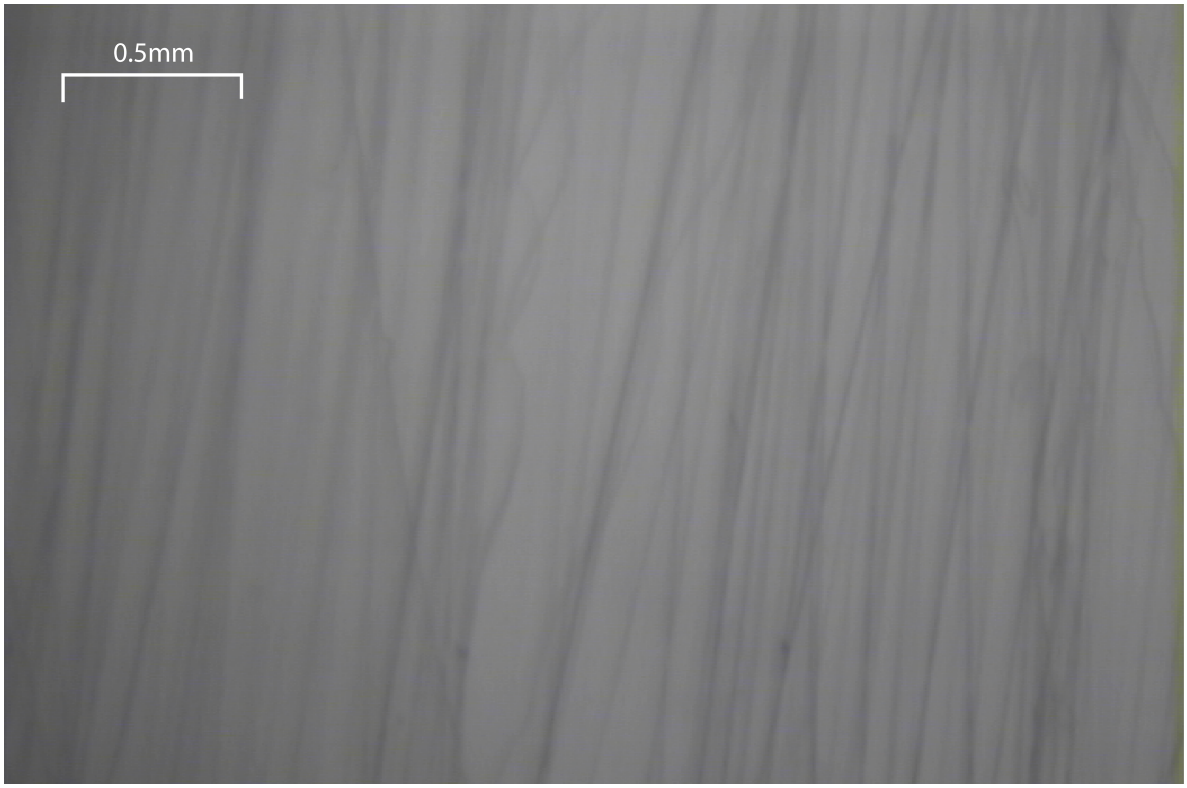

Figure 3.8: Optical Microscope image of neat PLLA fiber sample. The image is an unpolarized reflection image taken under white light illumination.

Performing AFM in the less dense regions of the sample revealed smaller fibers anywhere between 80nm-700nm in diameter. The optical image shows us that the fiber lengths were very long relative to their diameters, and AFM height images (Fig 3.9) showed that the diameter of the fibers were uniform on the measured area and had a smooth topology.

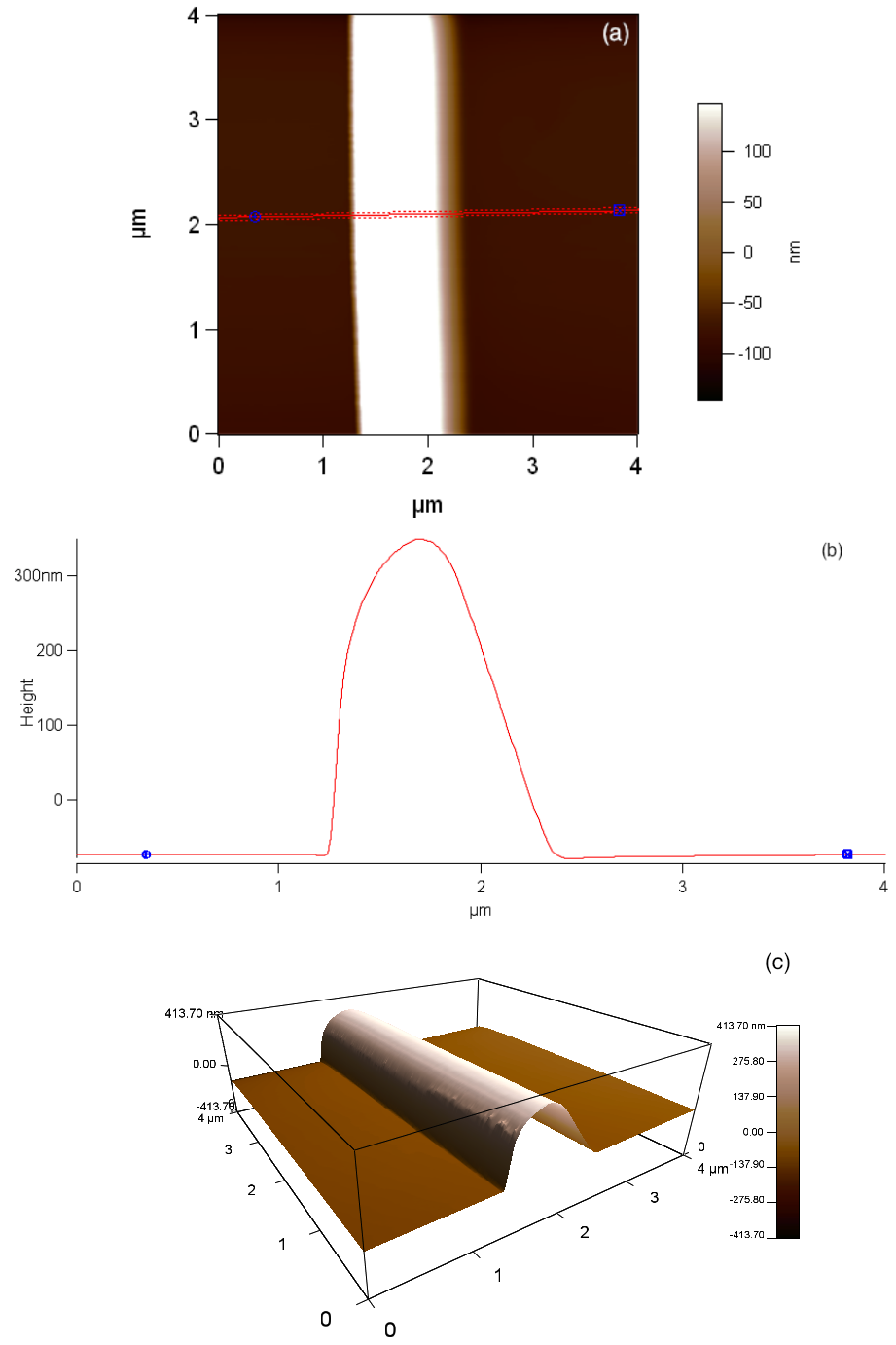

Figure 3.9: The topography of a neat PLLA fiber. a) AFM Height retrace, measuring the height of the sample surface, with the red line indicating the line section that was analyzed to produce the adjacent graph. The fiber in this image runs through the middle from top to bottom. b) A graph of the height of the fiber across the line section perpendicular to the fiber axis, showing the cylindrical cross section of the fiber. Note the fiber width exceeds the height as the width also measures the radius of the tip, ~50 nm in our case. c) A 3D rendering of the height map in a) showing the uniform diameter of the fiber.

3.3.2 Measurements of the Transverse Dielectric Constant of Neat PLLA Fibers

Fibers with diameters of around 300 nm were targeted and measured with EFM as the methods section outlines. In order to calculate the dielectric constant of the fiber ε_f, the relative negative phase-shift of the tip-fiber + substrate system must be measured. Fig(3.10) shows how this was achieved, by measuring the relative phase shift between the substrate and the fiber at a point where its linear thickness is greatest. More specifically, the difference in value of the lowest point of the phase graph and a baseline point (one that is far from the fiber on the flat part of the graph) was taken. This phase shift corresponded to the phase shift in eq 2.11. Recall that this equation only held for small absolute phase shifts (~30 degrees), so for larger absolute phase shifts eq 2.10 was used, by taking the phase shift over the substrate and the phase shift over the fiber and substrate, and plugging them into the equation directly.

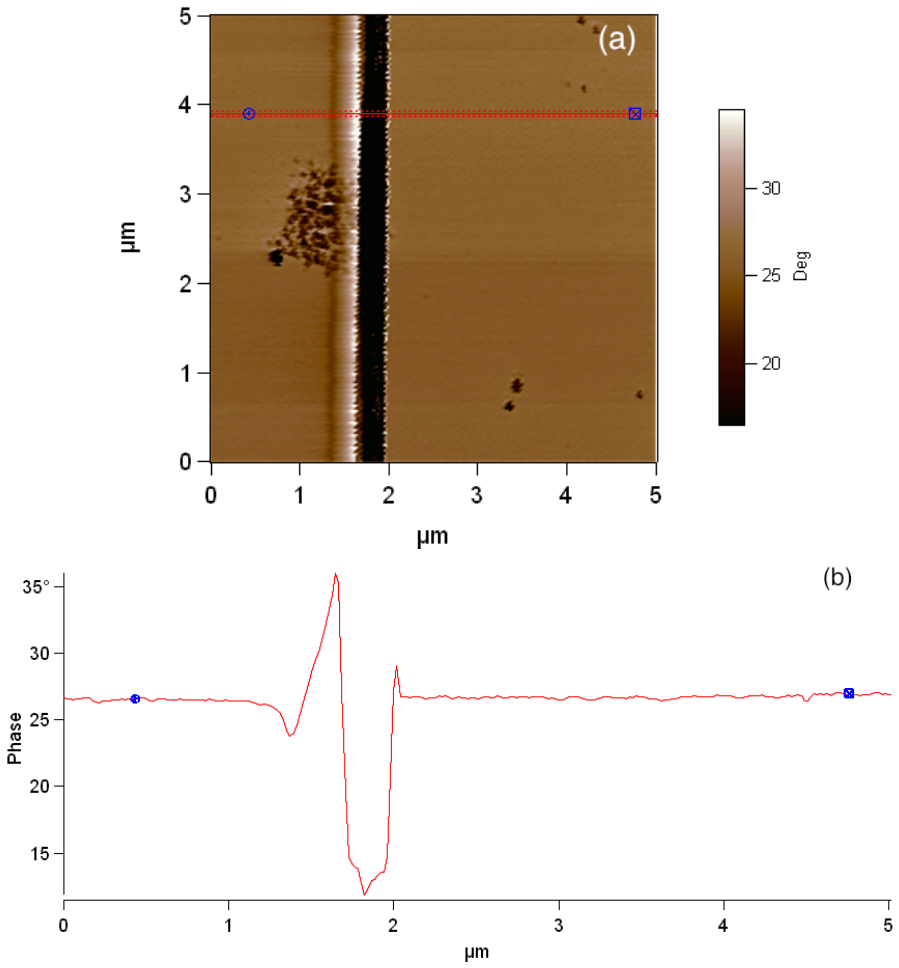

Figure 3.10: Measurements of the phase of oscillation under EFM at 6 V of a neat PLLA fiber. a) Phase map of the whole fiber. Changes in the phase are observed that run along the length of the fiber. A red line shows the location of the line scan used to produce the image below. b) A graph of the phase of the tip oscillation across a line section perpendicular to the fiber axis. The relative phase is taken to be the difference in value between the tip-substrate phase shift and the tip-substrate&fiber system. The blue circular marker indicates the reference point used to measure the tip-substrate phase shift. The blue square marker indicates the reference point used to calculate the negative phase shift corresponding to the tip-substrate&fiber system (annotated for clarity). For large absolute phase shifts we cannot use the small angle approximation and must use the absolute values of both phase shifts inserting them into eq 2.10

Phase shifts were measured across the same part of a fiber for multiple voltages in order to verify the linear trend between the tangent of the phase shift and the tip voltage squared (Fig 3.11), as described by eq 2.10. A linear regression was applied to the set of phase shifts and the gradient was extracted to give a value of the constant of proportionality of the linear relation, and thus a value for $\left(C_2'' - C_1''\right)$ as Q and k are measured.

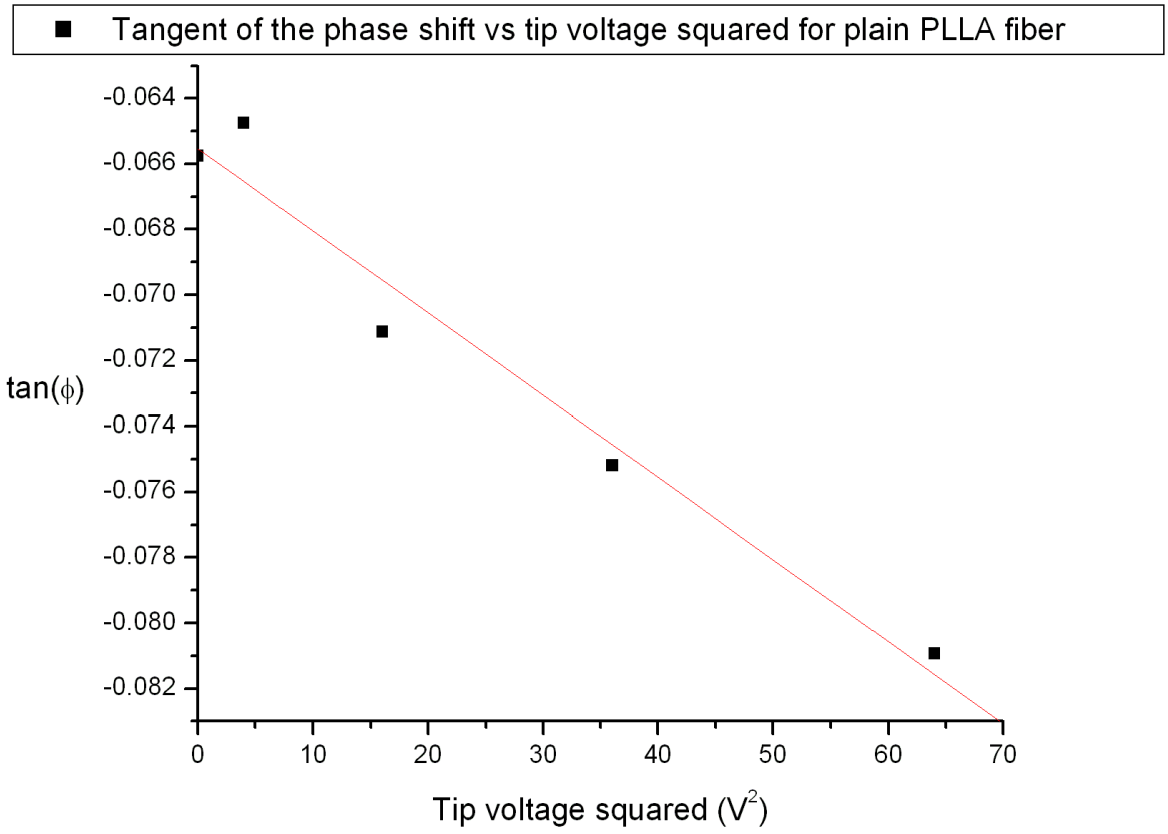

Figure 3.11: The linear relation between the tangent of the relative phase shift of the tip oscillation as measured in Fig(3.10), and the tip voltage squared.

Using this calculated value, $C_1^{''}$ can be calculated from experimental parameters (eq 2.12) allowing us to calculate $C_2^{''}$, and then eq 2.13 can be inverted to give the dielectric constant of the fiber, ε_f in terms of $C_2^{''}$ and experimental parameters:

$$\varepsilon_f = \left(\sqrt[3]{\frac{2\varepsilon_0 \pi R_{tip}^2}{C_2^{''}}} - h - \frac{t}{\varepsilon_s} \right)^{-1} D \tag{3.1}$$

For individual fibers, the relation between phase shift and tip voltage was measured for multiple line segment locations across the length of the fiber, each one perpendicular to the fiber axis. From each of these measured slopes, the value of the dielectric constant was calculated. Preliminary measurements of an individual PLLA fiber produced a distribution of dielectric constants (Fig 3.12).

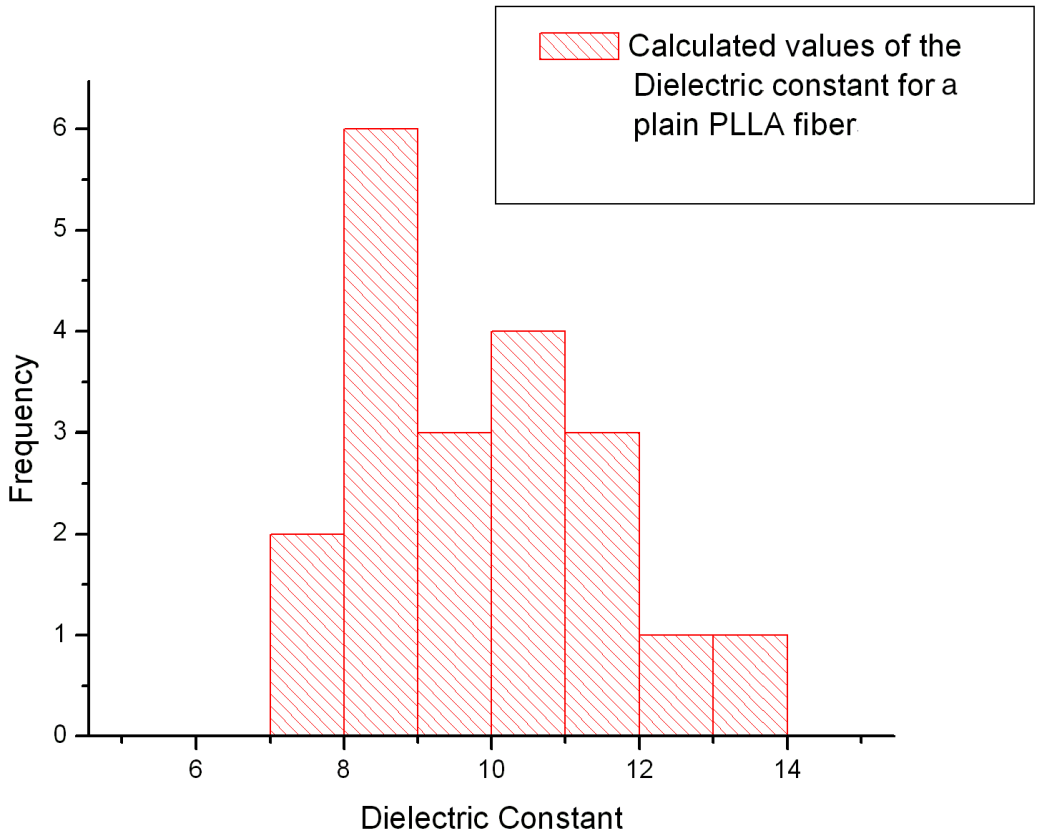

Figure 3.12: Histogram of measured ε_f values for an individual neat PLLA fiber. Modeled as a gaussian, the distribution has a mean value of 9.8 and a standard deviation of 1.7

Such a value of the dielectric constant is very high for a polymer, typical values for polymers lie in the range 2.0-3.0.[17] The discrepancy might be explained as a breakdown of the modeling equations of the system, as the last chapter suggests.

3.4 PLLA Fibers with Embedded MW CNTs

3.4.1 MW CNT Embedded PLLA Fiber Topography

The treatment of the MW CNT embedded PLLA nanofibers was very similar to that of the neat fibers. The optical microscope revealed similar fiber diameters to the neat fibers (Fig 3.13), and AFM confirmed the presence of smaller fibers with diameters in the range 100 nm-1000 nm.

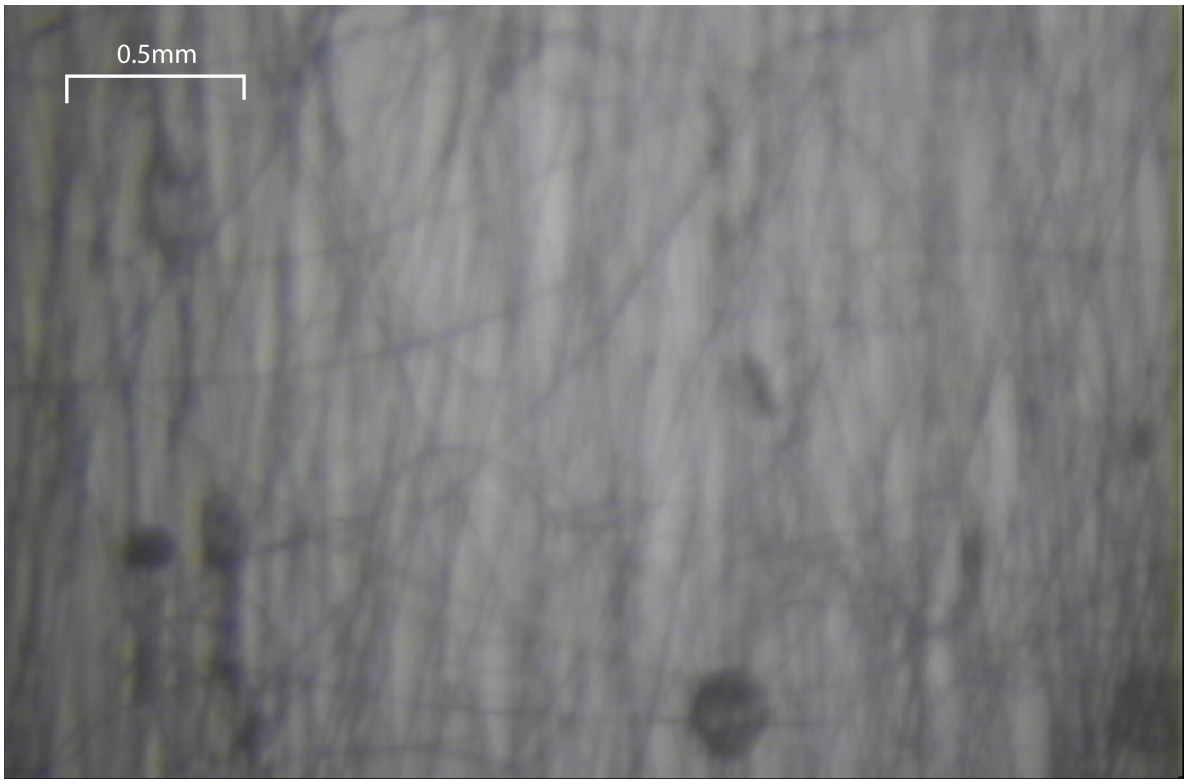

Figure 3.13: Optical microscope image of MW CNT embedded PLLA fibers

Since it is entirely possible for a neat fiber to be created in the electrospinning process. A challenge to overcome in this experiment is choosing fibers that actually have CNTs in them. Since neat fibers and CNT embedded fibers cannot be distinguished by eye, or even a preliminary EFM scan, instead only larger fibers (diameter $\geq$300 nm) were measured. The reasoning behind this was that we expect MW CNTs themselves to have diameters on the order of 100 nm and so smaller fibers were very unlikely to contain a CNT, however larger fibers could very easily house one or even multiple CNTs.

Once again the topology of these fibers was found to be rather smooth, and the diameter consistent along the length of the scan (Fig 3.14).

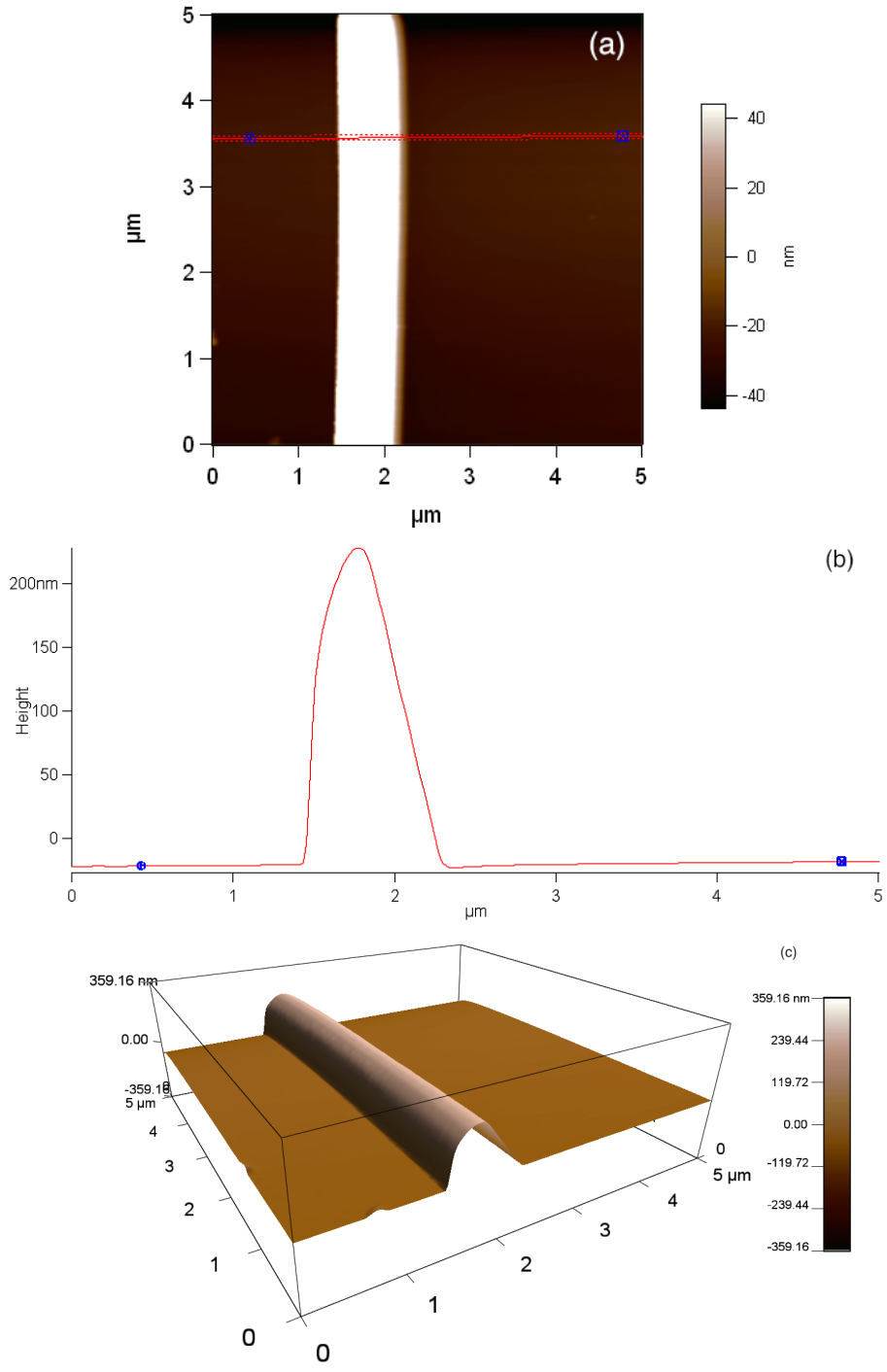

Figure 3.14: The topography of a composite PLLA fiber. a) AFM Height retrace, measuring the height of the sample surface, with the red line indicating the line section that was analyzed to produce the adjacent graph. The fiber in this image runs through the middle from top to bottom. b) A graph of the height of the fiber across the line section perpendicular to the fiber axis, showing the cylindrical cross section of the fiber. c) A 3D rendering of the height map in a) showing the uniform diameter of the fiber.

3.4.2 Measurements of the Transverse Dielectric Constant of MW CNT Embedded PLLA Fibers

To measure the dielectic constant of composite fibers an identical method was employed as in the neat fiber case. EFM was performed on the composite fibers to measure the relative phase shift of the tip-fiber system. (Fig 3.15).

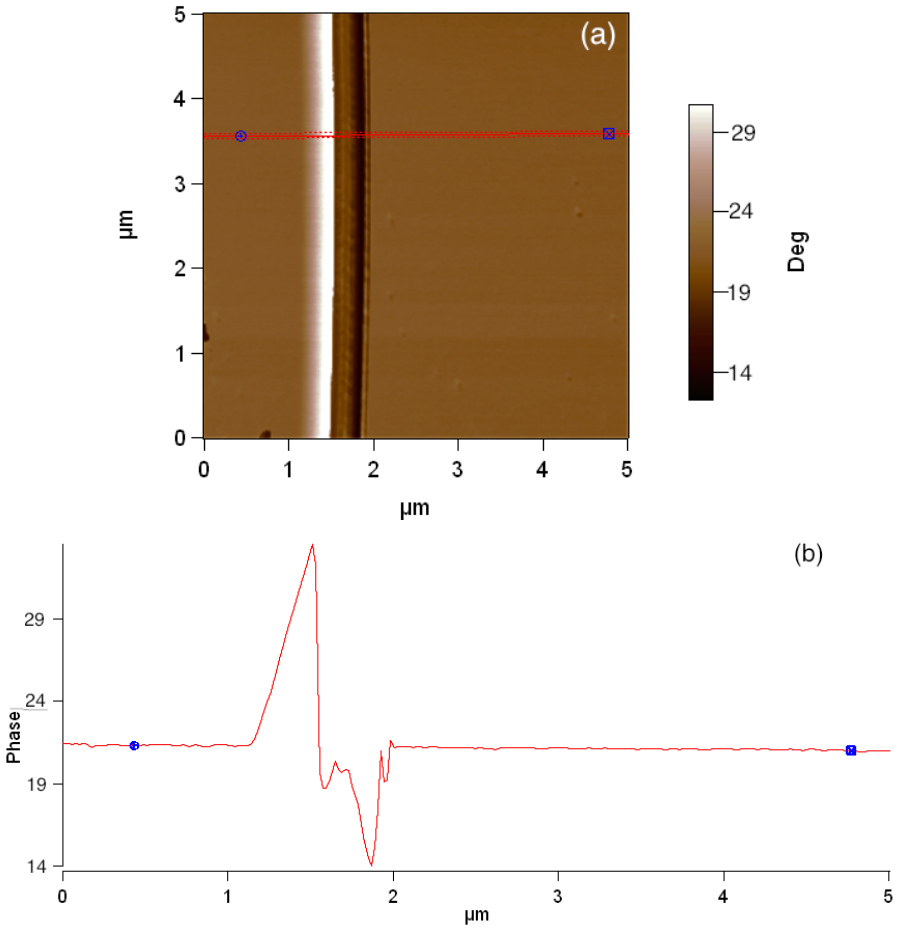

Figure 3.15: Measurements of the phase of oscillation under EFM at 6 V of a composite PLLA fiber. a) Phase map of the whole fiber. Changes in the phase are observed that run along the length of the fiber. A red line shows the location of the line scan used to produce image below. b) A graph of the phase of the tip oscillation across a line section perpendicular to the fiber axis. The relative phase is taken to be the difference in value between the tip-substrate phase shift and the tip-substrate&fiber system. The blue circular marker indicates the reference point used to measure the tip-substrate phase shift. The blue square marker indicates the reference point used to calculate the negative phase shift corresponding to the tip-substrate&fiber system.

For these fibers, a similar analysis was performed as for the neat fibers. The phase shift across a

line segment of the fiber at a specific location was measured across multiple images of the same fiber scanned at different tip voltages. The tangent of these phase shifts were then plotted against the tip voltage squared to find a linear relation. However attempts to calculate a dielectric constant for the composite fibers failed to yield results.

Chapter 4

Conclusions

4.1 Discussion of Results

The initial experiment turned out to be much more complicated than originally thought. The equation modeling the system was very sensitive to input parameters, and deviations from the simple tip-sample model were detected.

Further analysis of the equation modeling the tip-sample system as a parallel plate capacitor problem (Eq 2.13) showed that the calculated values of ε_f were extremely sensitive to the parameters of the equation, in particular Q, the quality factor of the tip oscillation, and k, the tip spring constant. Q was measured to high accuracy, however k was provided by the manufacturer with a large range of values. Thus two methods, one new and one old, were explored to measure k and were shown to get the value to a degree of accuracy sufficient to preventing a large scope of error on the calculated value of ε_f . The two methods yielded distinct results that were in the manufacturer specifications. As a result the thermal method was used for the project.

EFM scans of the phase of the tip oscillation revealed phenomena that could not be explained by the physical model used by this project to study the tip-sample interaction. First, transient forces on the tip as it scanned the sides of the fiber led to cantilever oscillations not described by simple harmonic motion, the so called cross-talk of the system. A second more problematic phenomenon was observed as a hysteresis of the tip phase as it passed over a fiber during EFM, indicating that the process in EFM permanently partially polarizes the fiber such that long range tip-fiber forces still affect the motion of the cantilever even once the tip has passed the fiber.

Despite the difficulties and deviations from the model, preliminary measurements of the dielectric constant of both the neat fibers were made, and attempts at the composite fibers were made. However the results still deviated from expected values and so this suggests once more that the appropriate physics of the system is not captured by the simple model of the tip-fiber system proposed.

4.2 Future Work

The next step of this project is to perform a detailed analysis of fiber-tip interactions, and develop a model that goes beyond the simple parallel plate capacitor and also includes the distribution of dipoles in the fiber. This would be done using tips with more accurate specifications. Furthermore a model would be made of the hysteresis of the system. If the hysteresis is due partial polarization of the fiber this can be overcome by performing EFM under an AC tip voltage[18] rather than a DC bias. Once these models are obtained, more measurements can be made of neat PLLA fibers and composite PLLA fibers so that their respective dielectric constant can be measured, and compared to one another so that we can observe any differences between them. With this comparison in mind, the next step would be to perform EFM on pure multiwall carbon nanotubes, so the composite fiber system could be analyzed for the combination of the properties of the neat PLLA fiber and the MW CNTs alone.

Bibliography

[1] M. S. D. Riichiro Saito, Gene Dresselhaus, *Physical properties of carbon nanotubes.* Imperial College Press, 1998.

[2] J. R. F. Leslie Y. Yeo, "Electrospinning carbon nanotube polymer composite nanofibers," *Journal of Experimental Nanoscience*, vol. 1, pp. 177–209, June 2006.

[3] V. Mittal, ed., *Polymer Nanotube Nanocomposites: Synthesis, Properties, and Applications.* Scrivener Publishing LLC, 2010.

[4] A. Vilalta-Clemente and K. Gloystein, "Principles of atomic force microscopy," *Physics of Advanced Materials Winter School*, 2008.

[5] J. Stettner, *Self assembled monolayer formation of alkanethiols on gold: Growth from solution versus physical vapor deposition.* PhD thesis, Graz University of Technology, 2010.

[6] N. J. P. Cristian Staii, Alan T. Johnson Jr, "Quantitative analysis of scanning conductance microscopy," *Nano Letters*, vol. 4, pp. 859–862, February 2004.

[7] Asylum Research inc, *EFM on the MFP-3D: Operations manual provided by Asylum Research inc.*

[8] P. Girard, "Electrostatic force microscopy: principles and some applications to semiconductors," *Nanotechnology*, vol. 12, pp. 485–490, 2001.

[9] I. S. C. Audrey Frenot, "Polymer nanofibers assembled by electrospinning," *Current Opinion in Colloid and Interface Science*, vol. 8, pp. 64–75, 2003.

[10] S. K. A. L. Yarin and D. H. Reneker, "Taylor cone and jetting from liquid drolets in electrospinning nanofibers," *Journal of Applied Physics*, vol. 90, November 2001.

[11] W. <http://upload.wikimedia.org/wikipedia/commons/7/79/Polylactides_Formulae_V.1.svg>, "Polylactides formulae v.1 (online)."

[12] ""structure of lactides" http://www.futerro.com/images/lactide1.jpg (online)."

[13] M. P. S. L. D. X. W. Minoo Naebe, Tong Lin, "Electrospun single-walled carbon nanotube/polyvinyl alcohol composite nanofibers: structure–property relationships," *IOP Nanotechnology*, vol. 19, May 2008.

[14] E. M. K. E. H. V. M. John H. Lehman, Mauricio Terrones, "Evaluating the characteristics of multiwall carbon nanotubes," *Carbon*, vol. 49, pp. 2581–2602, March 2011.

[15] B. Stojetz, *Interplay of Bandstructure and Quantum Interference in Multiwall Carbon Nanotubes*. PhD thesis, Universitat Regensburg, 2004.

[16] B. S. Cagdas D. Onal and M. Sitti, "Cross-talk compensation in atomic force microscopy," *Review of Scientific Insruments*, vol. 79, no. 10, 2008.

[17] *Zulkifli Ahmad (2012). Polymer Dielectric Materials, Dielectric Material, Dr. Marius Alexandru Silaghi (Ed.), ISBN: 978-953-51-0764-4, InTech, DOI: 10.5772/50638. Available from: http://www.intechopen.com/books/dielectric-material/polymer-dielectric-materials.*

[18] <https://support.asylumresearch.com/forum/showthread.php|%3f1440-Applying-an-AC-bias-to-the-tip-during-a Nap-pass|&highlight=EFM+large+phase+shift>, "Asylum research forums."